



Original Full Length Article

Periostin expression contributes to cortical bone loss during unloading

Maude Gerbaix ^a, Laurence Vico ^b, Serge L. Ferrari ^a, Nicolas Bonnet ^{a,*}^a Division of Bone Diseases, Department of Internal Medicine Specialties, Geneva University Hospital & Faculty of Medicine, Geneva 14, Switzerland^b Institut National de la Santé et de la Recherche Médicale (INSERM), Unité 1059, Laboratoire de Biologie Intégrée du Tissu Osseux, Université de Lyon, St-Etienne, France

ARTICLE INFO

Article history:

Received 19 June 2014

Revised 19 September 2014

Accepted 15 October 2014

Available online 23 October 2014

Edited by: David Fyhrie

Keywords:

Periostin

Sclerostin

Unloading

Cortical

Bone formation

ABSTRACT

Periostin (a product of *Postn* gene) is a matricellular protein which is increased in periosteal osteoblasts and osteocytes upon mechanical stimulation. We previously reported that periostin-deficient mice (*Postn*^{-/-}) have low bone mass and a diminished response to physical activity due to a lack of sclerostin (a product of *Sost* gene) inhibition by mechanical loading. Here we hypothesized that periostin could play a central role in the control of bone loss during unloading induced by hindlimb suspension (HU).

In *Postn*^{+/+} mice (wildtype littermate), HU significantly decreased femur BMD, as well as trabecular BV/TV and thickness (Tb.Th). Cortical bone volume and thickness at the femoral midshaft, also significantly decreased. These changes were explained by an inhibition of endocortical and periosteal bone formation activity and correlated with a decrease of *Postn* expression and a consecutive increase in *Sost* early after HU. Whereas trabecular bone loss in *Postn*^{-/-} mice was comparable to *Postn*^{+/+} mice, HU did not significantly alter cortical bone microstructure and strength in *Postn*^{-/-} mice. Bone formation remained unchanged in these mice, as *Sost* did not increase in the absence of periostin. In contrast, changes in *Dkk1*, *Rankl* and *Opg* expression in response to HU were similar to *Postn*^{+/+} mice, indicating that changes in periostin expression were quite specifically related to changes in *Sost*. In conclusion, HU inhibits periostin expression, which in turn plays an important role in cortical bone loss through an increase in *Sost*. These results further indicate that periostin is an essential mediator of cortical bone response to mechanical forces (loading and unloading).

© 2014 Elsevier Inc. All rights reserved.

Introduction

Weightlessness and immobility, as experienced by bedridden, immobilized patients or astronauts, lead to a reduction in bone mass and strength. Skeletal adaptation to unloading involves a continuous reduction in bone formation rate but also a precocious and transient increase in bone resorption [1,2]. Osteocytes orchestrate mechanotransduction in bone, as their ablation diminishes the bone response to loading [3]. Among the osteocytic molecules involved in mechanotransduction, sclerostin plays a major role through the inhibition of Wnt/ β -catenin signaling [4–7]. Hence sclerostin gene (*Sost*) expression is inhibited by loading, which leads mainly but not exclusively to an increase in bone formation [8,9]. In accordance, SOST expression increases with unloading [8]. In addition to its prominent inhibitory effects on bone formation, some *in vitro* and *in vivo* studies suggest that sclerostin also stimulates bone resorption by decreasing the OPG/RANKL ratio in osteoblasts and osteocytes [9]. Thus, *Sost*-deficient mice are resistant to bone loss induced by hindlimb suspension, although the contribution of bone formation and/or bone resorption in this model remains

unclear [5]. Accordingly, pharmacological inhibition of sclerostin restores bone formation in different models of microgravity, i.e., tail suspension, immobilized rats, and spine injury model [10–13]. We previously reported that down regulation of SOST and cortical bone formation in response to mechanical loading and parathyroid hormone (PTH) depends on the expression of a matricellular protein, periostin, the expression of which is increased in these conditions [14,15]. In turn, periostin triggers β -catenin mediated signaling [15]. Noteworthy, β -catenin mediated the stimulation of OPG expression in osteocytes [16], raising the possibility that periostin could also be involved in the control of bone resorption by these cells. In addition, periostin is implicated in tissue regeneration and repair mechanisms, which has been previously described in the lungs and heart [17]. Besides, periostin expression is increased by inflammation and mechanical stress, suggesting a potential function of this molecule in maintaining the structure and integrity of connective tissues. Periostin binds to integrins α v β 3 and α v β 5, regulating cell adhesion and mobility [18,19] and promotes cell survival via the Akt/protein kinase B pathway. These observations clearly suggest that periostin could be a key role in skeletal adaptation to unloading. We hypothesized that unloading would reduce periostin expression, which in turn might contribute to increasing *Sost* and decreasing OPG, and thereby control the detrimental effects of unloading on bone. More specifically, in the absence of periostin,

* Corresponding author at: 64 Av de la Roseraie, 1205 Geneva 14, Switzerland.
Fax: +41 223829973.

E-mail address: nicolas.bonnet@unige.ch (N. Bonnet).

bone mineral density (BMD), structure and bone formation decrease would be attenuated.

In order to test this hypothesis, we characterized bone mass, microarchitecture and strength in response to 7 and 21 days of hindlimb unloading (HU) in *Postn*^{-/-} and *Postn*^{+/+} mice. In *Postn*^{+/+}, cortical and trabecular bone loss were proportionated, whereas in *Postn*^{-/-} bone loss occurred exclusively in the trabecular compartment. In *Postn*^{+/+}, *Postn* mRNA decreased at 7 and 21 days, whereas *Sost* increased only at 7 days with unloading. These changes were paralleled by a sustained inhibition of bone formation, particularly in the cortical compartment, and also by a transient increase in osteoclast number. In the absence of periostin regulation by unloading in *Postn*^{-/-} mice, cortical bone formation was maintained, especially in the periosteum.

Materials and methods

Animals

To generate *peri^{lacZ}* knock-in mice, Rios et al. generated a replacement-targeting vector, where the bacterial β -galactosidase gene was knocked into the *periostin* gene locus [20], so that the Lac Z reporter was expressed instead of periostin under the control of the periostin promoter. They infected 129SvJ mouse embryonic stem (ES) with this vector and generated chimeras by microinjection of ES using standard protocols. Chimeras were subsequently bred with C57BL/6 to generate heterozygotes. These were subsequently backcrossed for 10 generations, resulting in a genome of 99% C57BL/6J. Mice were singly housed 2 weeks before initiation of unloading, maintained under standard conditions and had access to water and soft diet *ad libitum* (Harlan Teklad 2019, SDS, England). Soft diet had been chosen to reduce the malnutrition of the *Postn*^{-/-} mice observed under standard diet due to the enamel and dentin defects of the incisors and molars [20].

Three-month-old male *Postn*^{-/-} and *Postn*^{+/+} mice were subjected to 7 or 21 days of unloading ($n = 8$ per genotype for unloading group and $n = 6$ for controls). HU was achieved by tail suspension as previously described [2]. The height of the mice hindquarters was adjusted to prevent any contact of the hindlimbs with the cage floor, resulting in approximately a 30° head-down tilt. The forelimbs of the animals maintained contact with the cage bottom, allowing the mice full access to the entire cage. Normal weight-bearing mice (Control) were also singly housed.

To measure dynamic indices of bone formation, mice received subcutaneous injections of calcein (25 mg/kg, Sigma, Buchs, Switzerland) 7 and 2 days before euthanasia. Animal procedures were approved by the University of Geneva School of Medicine Ethical Committee and the State of Geneva Veterinary Office.

In vivo measurement of BMD

Total body, femoral and spinal BMD (g/cm²) were measured *in vivo* by dual-energy X-ray absorptiometry (PIXImus2, GE lunar, Madison WI) [21] before initiation of tail suspension and just before euthanasia, i.e., after 7 and 21 days of unloading.

Ex vivo measurement of microarchitecture

Micro-computed tomography (microCT UCT40, Scanco Medical AG, Basserdorf Switzerland) was used to assess trabecular bone volume fraction in the distal femur, and cortical bone geometry at the midshaft femur diaphysis, as previously described [14]. Briefly, trabecular and cortical bone regions were evaluated using isotropic 12 μ m voxels.

For the trabecular region, to eliminate the primary spongiosa, we analyzed 100 slices starting from 50 slices below the distal growth plate.

Femoral cortical geometry was assessed using 50 continuous CT slides (600 μ m) located at the midshaft. Images were segmented using a fixed threshold approach. Morphometric variables were computed

from binarized images using direct, three-dimensional techniques that do not rely on prior assumptions about the underlying structure [22]. For the trabecular bone regions, we assessed bone volume fraction (BV/TV, %), trabecular thickness (TbTh, μ m), trabecular number (TbN, mm⁻¹), trabecular connectivity density (Tb Conn Density, mm⁻³), and structural model index (SMI). The latter was measured to determine the prevalence of plate-like or rod-like trabecular structures, where 0 represents “plates” and 3 “rods” [22]. For cortical bone at the femoral midshaft, we measured cortical tissue volume (CtTV, mm³), bone volume (CtBV, mm³), marrow volume (BMAV, mm³), and average cortical width (CtTh, μ m).

RNA extraction and quantitative PCR

The whole tibia was excised; both tibial extremities were cut and diaphysis was flushed with cold PBS to separate the bone marrow from the cortex. Tibial diaphyses were immediately pulverized to a fine powder and homogenized in peqGold Trifast (peQLab Biotechnologie GmbH) using FastPrep System apparatus (QBiogene) in order to achieve quantitative RNA extraction. Total RNA was extracted and then purified on mini-columns (RNeasy Mini kit, Qiagen) in combination with a deoxyribonuclease treatment (RNase-free DNase Set, Qiagen) to avoid DNA contamination.

Single stranded cDNA templates for quantitative real-time PCR (qRT-PCR) analyses were carried out using SuperScript III Reverse Transcriptase (Invitrogen AG, Basel) following the manufacturer's instructions. Quantitative RT-PCR was performed using predesigned TaqMan® Gene Expression Assays (references in Table S1). A Biomek 2000 robot (Beckman Coulter, Nyon, Switzerland) was used for liquid handling (10 μ l) in 384-well plates with 3 replicates per sample. The cDNA was PCR amplified in a 7900HT SDS System and raw threshold-cycle (Ct) values were obtained from SDS 2.0 software (Applied Biosystems, Rotkreuz, Switzerland). Relative quantities (RQ) were calculated with the formula $RQ = E^{-Ct}$ using an efficiency (E) of 2 by default. For each gene the highest quantity was arbitrarily designated a value of 1.0. The mean quantity was calculated from triplicates for each sample and this quantity was normalized to the similarly measured mean quantity of the *GAPDH* normalization gene. Finally, normalized quantities were averaged to 4 animals and represented as mean \pm SEM (Table S1).

Histomorphometry

To measure dynamic indices of bone formation, mice received subcutaneous injections of calcein (10 mg/kg, Sigma, Buchs, Switzerland) 7 and 2 days before euthanasia. Femurs were embedded in methyl methacrylate (Merck, Switzerland), and 8- μ m-thick transversal sections of the midshaft were cut with a Polycot E microtome (Leica Corp. Microsystems AG, Glattburg, Switzerland) and mounted unstained for evaluation of fluorescence. 5- μ m thick sagittal sections were stained with modified Goldner's trichrome, and histomorphometric measurements were performed on the secondary spongiosa of the proximal tibia metaphysis and on the endocortical and periosteal bone surfaces in the middle of the tibia, using a Leica Corp. Q image analyzer at 40 \times magnification. All parameters were calculated and expressed according to standard formulas and nomenclatures [23]: mineral apposition rate (MAR, μ m/day), single labeled surface (sLS/BS, %), and double-labeled surface (dLS/BS, %), mineralizing perimeter per bone perimeter (MPm/BPm, %). Mineralizing surface per bone surface (MS/BS, %) was calculated by adding dLS/BS and one-half sLS/BS. Bone formation rate (BFR/BS, μ m³/ μ m²/day) was calculated as the product of MS/BS and MAR.

TRAP was detected by using hexazotized pararosanilin (Sigma, St Louis, MO) and naphthol ASTR phosphate (Sigma, St Louis, MO) to reveal osteoclasts; non-osteoclastic acid phosphatase was inhibited by adding 100 mMol/l L(+)-tartric acid (Sigma, St Louis, MO) to

the substrate solution. The following parameters were recorded: the number of TRAP + osteoclasts in contact with trabeculae (N.Oc/BPm; expressed in cells per millimeter of trabecular bone surface) and the osteoclast surface (Oc.S/BS; expressed in %).

Testing of mechanical resistance

The night before mechanical testing, bones were thawed slowly at 7 °C and then maintained at room temperature. The length of the femur was measured using callipers with an integrated electronic digital display and the midpoint of the shaft was determined. The femur then was placed on the material testing machine on two supports separated by a distance of 9.9 mm and load was applied to the midpoint of the shaft, thus creating a three-point bending test. The mechanical resistance to failure was tested using a servo-controlled electromechanical system (Instron 1114, Instron Corp., High Wycombe, UK) with actuator displaced at 2 mm/min. Ultimate force (maximal load, measured in Newtons [N]), stiffness (slope of the linear part of the curve, representing the elastic deformation, N/mm), and energy (surface under the curve, N*mm) were obtained from the load-displacement curve.

Data analysis

We first tested the effects of unloading within groups (*Postn*^{-/-} and *Postn*^{+/+}) by paired or unpaired *t*-tests. To compare the effect of genotype and the response to unloading, we used a 2 × 2 ANOVA. The *p* of interaction between the genotype and unloading was only mentioned when it was found to be significant (*p* < 0.05). As appropriate, post hoc testing was performed using Fisher's protected Least Squares Difference (PLSD). Data are presented as mean ± SEM.

Results

Unloading decreased *Postn* and *Sost* increase attenuated in the absence of *Postn*

After 7 days of HU, *Postn* gene expression was reduced (-24% vs. control mice, *p* < 0.05), whereas *Sost* expression levels were increased (+111% vs. control mice, *p* < 0.01) (Fig. 1A). Unloading also significantly decreased *Sp7* and *Opg* gene expression without significant changes in *Rankl* mRNA. In *Postn*^{-/-} mice, *Sost* expression increased by 41% in response to HU (*p* < 0.05 vs. control mice) but was attenuated compared to *Postn*^{+/+} mice (+111%, above), and *Sp7* was not affected by HU. Interestingly, however, *Dkk1* expression was increased by HU in *Postn*^{-/-}, but not in *Postn*^{+/+} mice, suggesting a compensatory mechanism that could explain why we also observed a decrease in *Opg* in the absence of periostin. After 21 days of HU, the same pattern of expression was observed for *Postn*, *Sost*, *Dkk1* and *Opg* (Fig. 1B), and *Rankl* expression significantly increased compared to ground control.

Postn^{-/-} mice partially protected against BMD loss by unloading

At baseline, *Postn*^{-/-} exhibited a significant lower body weight than *Postn*^{+/+} mice (22.9 ± 0.7 vs. 28.3 ± 0.7, respectively, *p* < 0.001). HU significantly decreased body weight after 7 days (*Postn*^{-/-} - 15.8% vs. controls, *p* < 0.05; *Postn*^{+/+} - 17.1% vs. controls, *p* < 0.05), with some recovery at 21 days (*Postn*^{-/-} - 7.0% vs. controls, *p* < 0.05; *Postn*^{+/+} mice - 14.4% vs. controls, *p* < 0.05) (Table 1, Fig. 2A). In *Postn*^{+/+} mice, 21 days of HU significantly decreased total body BMD and femoral BMD (-7.7% and -17.5% vs. controls, all *p* < 0.05). In *Postn*^{-/-}, the BMD decrease was about half that observed in *Postn*^{+/+} (total body BMD -4.2% vs. control, *p* = 0.08; femoral BMD -9.0% vs. control, *p* < 0.05) (Fig. 2A). Hence there was a significant interaction between *Postn* and unloading (*p* inter < 0.05 by a 2 × 2 ANOVA). In contrast, HU did not influence lumbar spine BMD (data not shown).

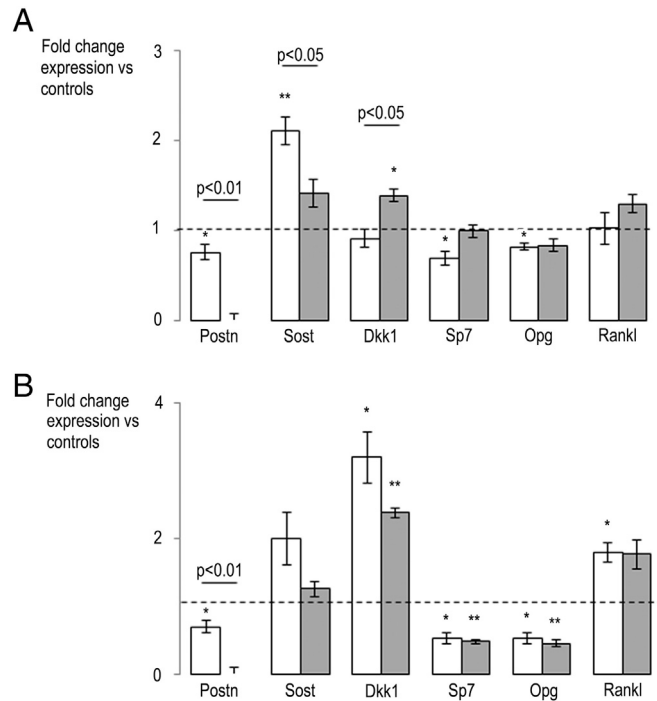


Fig. 1. Effects of 7 and 21 days of hindlimb unloading (HU) on osteoblastic gene expression in *Postn*^{+/+} and *Postn*^{-/-} mice. Bars show fold change expression in response to HU vs. controls (± sem) measured after 7 days (A) or 21 days (B) of unloading in *Postn*^{+/+} and *Postn*^{-/-} mice, respectively, white and gray bars. **p* < 0.05, ***p* < 0.01 unpaired *t*-test compared to sedentary group within periostin group; *p* < 0.05, *p* < 0.01 unpairing *Postn*^{+/+} and *Postn*^{-/-} response to HU by post hoc Fisher's PLSD following a two way ANOVA. *N* = 8 for hindlimb unloading groups and *n* = 6 for control groups.

Trabecular bone loss similar in *Postn*^{+/+} and *Postn*^{-/-}

After 7 days, unloading significantly decreased distal femur TbN and increased TbSp vs. control in both *Postn*^{+/+} and *Postn*^{-/-} (Table 1). This effect was associated with body weight loss for TbN (*r*² = 0.17, *p* < 0.05). At the vertebrae, trabecular microarchitecture parameters BV/TV and TbN tended to decrease, independently of periostin deficiency (Table 1). After 21 days of HU, BV/TV significantly decreased in *Postn*^{+/+} mice (-37.0% vs. controls, at both the distal femur and vertebrae), with a prominent decrease in trabecular thickness and increase in SMI, i.e., a more rod-shaped trabecular pattern in response to HU (Fig. 2B). Similar trends were observed in *Postn*^{-/-}, (BV/TV -26.9% and -20.7% vs. controls, respectively, at distal femur (*p* = 0.08) and vertebrae) (Fig. 2B, Table S2).

Cortical bone loss absent in *Postn*^{-/-} mice

After 7 days of HU, there were no significant changes in cortical microarchitecture (Table 1). However, after 21 days, CtBV had significantly decreased in *Postn*^{+/+} mice (-9.1% vs. control, *p* < 0.05). In contrast, no significant differences were observed between HU and control bones in *Postn*^{-/-} mice (Fig. 2C). Indeed, interaction between *Postn* and unloading on CtBV was significant (*p* < 0.05 by a 2 × 2 ANOVA). These periostin-dependent changes in the cortical bone response to HU were translated into significant differences in bone biomechanical properties, such as stiffness and elastic energy, which were significantly decreased in response to HU in *Postn*^{+/+} but not *Postn*^{-/-} mice (Fig. 2D).

Unloading decreased cortical bone forming indexes in *Postn*^{+/+} but not *Postn*^{-/-}

After 7 days of HU, trabecular bone forming indexes, i.e., MS/BS and BFR/BS, remained unchanged in both *Postn*^{-/-} and *Postn*^{+/+} (Table 1).

Table 1
Effect of 7 days of HU on femoral and vertebrae bone microarchitecture in *Postn*^{+/+} and *Postn*^{-/-}.

Parameters		<i>Postn</i> ^{+/+}		<i>Postn</i> ^{-/-}		P HU	P geno
		Controls	HU	Controls	HU		
Body composition	Body weight (g)	31.3 ± 1.3	23.7 ± 0.74 *	23.4 ± 1.0	19.3 ± 2.2	0.001	0.009
	Femur BMD (mg/cm ²)	58 ± 2	56 ± 2	57 ± 1	55 ± 2	0.45	0.61
Lumbar trabecular	BV/TV (%)	25.3 ± 1.1	19.0 ± 2.0	23.4 ± 1.9	21.7 ± 1.8	0.06	0.84
	Tb.Th (µm)	48 ± 1	46 ± 2	48 ± 2	49 ± 2	0.80	0.47
Femur trabecular	Tb.N	5.39 ± 0.08	4.46 ± 0.38	5.19 ± 0.17	4.59 ± 0.19	0.02	0.91
	Tb.Sp (µm)	0.176 ± 0.004	0.233 ± 0.022	0.186 ± 0.009	0.214 ± 0.010	0.02	0.80
Cortical	BV/TV (%)	7.5 ± 1.6	5.0 ± 1.6	7.5 ± 1.9	4.7 ± 1.2	0.11	0.91
	Tb.Th (µm)	39 ± 1	37 ± 2	39 ± 3	36 ± 1	0.11	0.85
Cortical	Tb.N	4.21 ± 0.28	3.31 ± 0.47	4.08 ± 0.24	3.44 ± 0.24	0.06	0.99
	Tb.Sp (µm)	0.240 ± 0.017	0.341 ± 0.048	0.249 ± 0.016	0.299 ± 0.020	0.06	0.65
	MAR (µm/day)	1.0 ± 0.08	0.83 ± 0.14	0.81 ± 0.04	0.96 ± 0.11	0.90	0.92
	MS/BS (%)	47.3 ± 4.3	35.0 ± 6.0	38.6 ± 7.1	31.0 ± 2.9	0.38	0.17
	BFR (µm ² /µm/day)	0.48 ± 0.08	0.33 ± 0.08	0.32 ± 0.07	0.33 ± 0.08	0.39	0.43
	Ct.density (HA/mm ³)	1202 ± 13	1160 ± 7	1188 ± 9	1171 ± 7	0.87	0.30
	CtTV (mm ³)	1.30 ± 0.04	1.21 ± 0.03	1.22 ± 0.06	1.10 ± 0.04	0.10	0.06
	CtBV (mm ³)	0.60 ± 0.03	0.58 ± 0.03	0.58 ± 0.01	0.54 ± 0.02	0.21	0.23
	CtTh (µm)	208 ± 5	208 ± 7	201 ± 8	199 ± 4	0.82	0.22

Hindlimb unloading (HU, n = 8 per genotype), controls (n = 6 per genotype), genotype (geno), *p < 0.05 unpaired t test compared to sedentary group within periostin group; p < 0.05, p < 0.01, p < 0.001 unpairing *Postn*^{+/+} and *Postn*^{-/-} mice by post-hoc Fisher's PLSD following 2 × 2 ANOVA. Bold data emphasize that P HU is < 0.05.

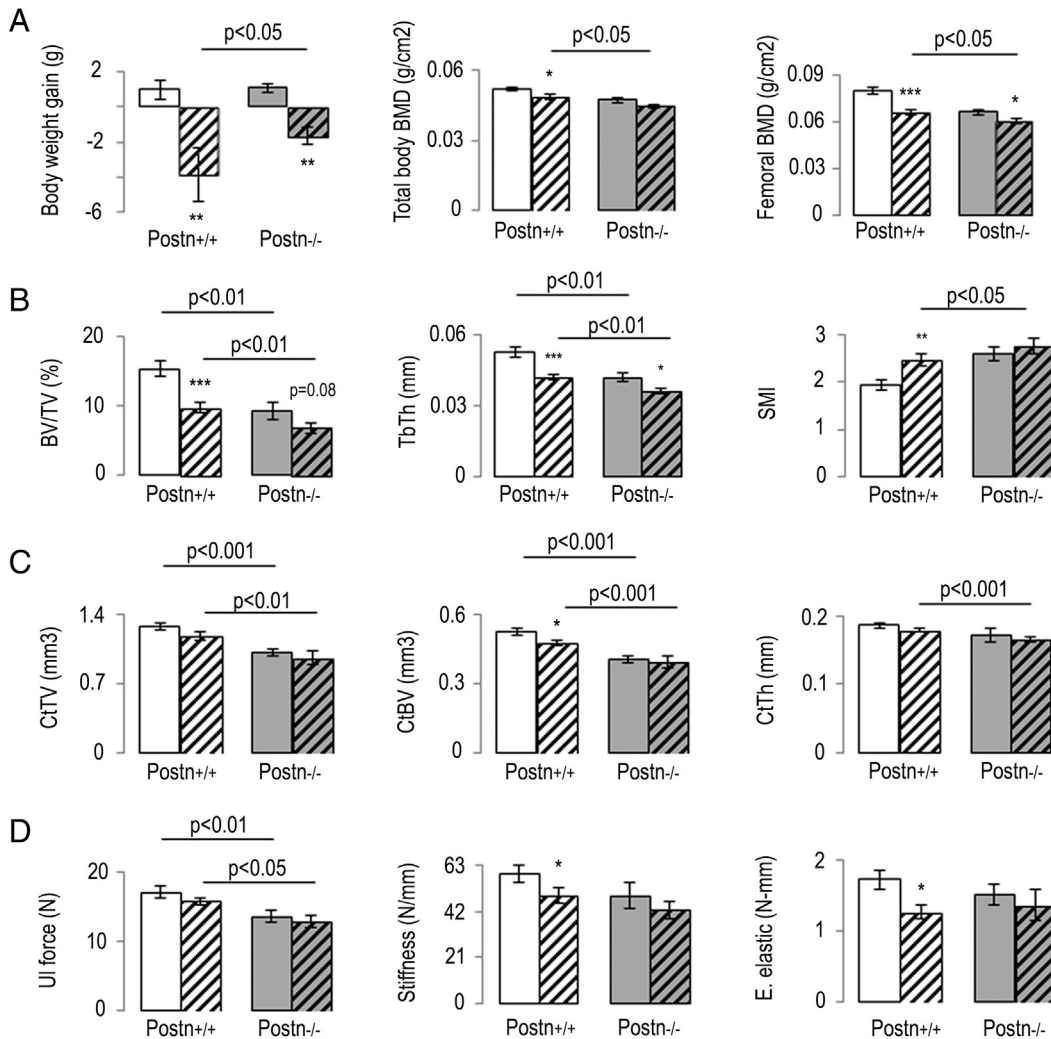


Fig. 2. Effects of 21 days of hindlimb unloading (HU) on body weight, bone mineral density (BMD), trabecular and cortical microarchitecture and bone strength in *Postn*^{+/+} and *Postn*^{-/-} mice. (A) Body weight and BMD evaluated by DXA. (B) Trabecular bone microarchitecture at the distal femur, bone volume on tissue volume (BV/TV, %), trabecular thickness (TbTh, µm), and structural model index (SMI). (C) Cortical bone microarchitecture at the midshaft femur, tissue volume (TV, mm³), cortical bone volume (CtBV, mm³), and cortical thickness (CtTh, mm). (D) Biomechanical properties evaluated by three-point bending, ultimate force (UI force, N), stiffness (N/mm) and energy (E.). Bars show mean (± sem) measured after 21 days of unloading (hatched bars) or sedentary (open bars) in *Postn*^{+/+} and *Postn*^{-/-} mice, respectively, white and gray bars. *p < 0.05, **p < 0.01, ***p < 0.001 unpaired t-test compared to sedentary group within periostin group; p < 0.05, p < 0.01, p < 0.001 unpairing *Postn*^{+/+} and *Postn*^{-/-} mice by post hoc Fisher's PLSD following two way ANOVA. N = 8 for HU groups and n = 6 for control groups.

In contrast, HU significantly decreased endocortical and periosteal BFR in *Postn*^{+/+} (−89% and −100% vs. control mice, respectively, $p < 0.05$ and $p < 0.001$), whereas no significant difference was observed in *Postn*^{−/−} mice (Table 2). This effect was mainly due to a decrease in MAR and MPm/BPm, respectively, at the periosteum and endocortical surfaces (Table 2).

After 21 days of HU, bone formation remained inhibited in *Postn*^{+/+} mice. At that time, endocortical MAR and Ps MPm/BPm were also decreased in *Postn*^{−/−}, whereas their periosteal MAR and BFR were not compared to controls (Table 2).

Unloading induced a sustained increase in osteoclast number in *Postn*^{−/−} mice

After 7 days of HU, trabecular osteoclast surface and number significantly increased in *Postn*^{−/−} (respectively, +216% and +370% vs. control, $p < 0.05$) and in *Postn*^{+/+} mice (respectively, +102% and +103% vs. control, $p < 0.05$). Osteoclast number and surface were actually higher in HU *Postn*^{−/−} vs. HU *Postn*^{+/+} mice (Fig. 3A). After 21 days of HU, *Postn*^{+/+} mice still tended to have higher osteoclast number and surface vs. controls, although the difference was not any more significant (Fig. 3B). In *Postn*^{−/−} mice, however, the higher osteoclast number remained significant 21 days after HU, +136% vs. controls ($p < 0.05$).

To explain this difference in osteoclast number between *Postn*^{−/−} and *Postn*^{+/+}, we performed gene expression analysis involved in osteoclastogenesis after 21 days of unloading. *Opg*, *Rankl* or *Ctsk* fold change expression vs. controls was not different between *Postn*^{+/+} and *Postn*^{−/−} mice. *Mmp13* and *Trap* increases in response to HU were significantly higher in *Postn*^{−/−} vs. *Postn*^{+/+} mice (Table 3).

Discussion

Mechanical unloading via tail-suspension resulted in deterioration of trabecular and cortical structures as well as suppression of periosteal and endocortical bone formation in *Postn*^{+/+} mice. These changes were accompanied by an early and persistent decrease in *Postn* expression and an increase in *Sost* (at 7 days), followed by *Dkk1* (at 21 days), whereas *Rankl/Opg* expression ratio increased progressively. These changes in expression of major molecular factors that regulate bone remodeling are indeed expected to induce observed changes of bone mass and structure that occurred upon tail suspension in *Postn*^{+/+} mice. Consistent with the role of periostin in the regulation of *Sost* expression [15], *Sost* did not significantly increase in response to unloading in periostin deficient mice. However, *Dkk1* increased similarly to *Postn*^{+/+}, and changes in *Opg* and *Rankl* were also similar

to *Postn*^{+/+} mice, indicating that in these conditions, periostin specifically regulates *Sost* expression in osteocytes. As a result, periosteal and endocortical bone formation rate remained unchanged in *Postn*^{−/−}, although at a low level, and cortical bone loss was prevented. It is important to point out that SOST is already high in *Postn*^{−/−} mice vs. *Postn*^{+/+} [14]. Therefore, while *Sost* expression increased (up to 1.5-fold) in *Postn*^{−/−} mice, it has no effect on mass and structure, since levels of *Sost* are already high and cortical structure low. In contrast, trabecular bone loss in response to unloading persisted even in the absence of periostin. Similar observations about the prominent role of periostin in cortical vs. trabecular compartments have been made in response to PTH and probably reflect the dominant expression of periostin in cortical vs. trabecular bone [14].

A relationship between periostin and unloading was first noticed during cardiac remodeling, since periostin gene and protein expression were modulated by the placement and removal of an aortic band [24]. We had previously reported that periostin is necessary for bone anabolic response to mechanical stimuli [14] and that periostin directly inhibits *Sost* expression through its integrin α V β 3 receptor [15,25,26]. Furthermore, we showed that periostin stimulates Wnt- β -catenin signaling [15]. The present work demonstrates that periostin is also involved in the response to unloading, i.e., its expression decreases, and that in the absence of periostin, the sclerostin increase in response to unloading is partially blocked. Hence, in the absence of periostin, the effects of HU on cortical bone structure and strength are reduced. A similar spatiotemporal response to unloading with weaker long bones and resistance to unloading-induced bone loss was reported upon targeted ablation of osteocytes [3]. In accordance, *Sost* knockout mice were resistant to mechanical unloading-induced bone loss by blocking decrease of bone formation [5]. Moreover, they showed that in contrast to *Postn*^{+/+} mice, Wnt/ β -catenin signaling was not altered by unloading in mutant mice.

Intuitively, the profound and sustained suppression of bone formation was correlated to the increase of the two main antagonists, *Sost* and *Dkk1*, which were transient and respectively involved at an early and late time point and therefore complementary. In contrast, periostin expression decreased after 7 days of HU and its relative expression remained low throughout 21 days of unloading, suggesting an additional direct role on the continuous decrease in bone formation. As previously demonstrated in response to PTH, periostin can regulate bone formation through the following: [1] a direct stimulation on Wnt- β catenin signaling; [2] an indirect stimulation of Wnt- β catenin through *Sost* inhibition; and [3] no canonical signaling pathways [15]. Interestingly, in the absence of periostin and an increase in *Sost*, we observed an early increase in *Dkk1* expression, suggesting that *Sost* and/or periostin may normally repress *Dkk1* expression. This hypothesis is

Table 2
Effect of 7 and 21 days of HU on bone modeling/remodeling indices in femur of *Postn*^{+/+} and *Postn*^{−/−} mice.

Parameters		<i>Postn</i> ^{+/+}		<i>Postn</i> ^{−/−}		P HU	P geno
		Controls	HU	Controls	HU		
7 days	Ps MAR (μ m/day)	0.63 \pm 0.12	n.d.***	n.d.	0.16 \pm 0.11	0.02	0.02 SS
	Ps BFR/BPm (μ m ² / μ m/day)	0.15 \pm 0.03	n.d.***	n.d.	0.12 \pm 0.08	0.08	0.08
	Ps MPm/BPm (%)	0.15 \pm 0.03	0.07 \pm 0.03	0.06 \pm 0.04	0.41 \pm 0.15	0.19	0.24 S
	Ec MAR (μ m/day)	0.72 \pm 0.16	0.36 \pm 0.18	0.21 \pm 0.11	0.26 \pm 0.16	0.46	0.15
	Ec BFR/BPm (μ m ² / μ m/day)	1.18 \pm 0.62	0.12 \pm 0.07*	0.40 \pm 0.20	0.16 \pm 0.11	0.02	0.15
21 days	Ec MPm/BPm (%)	0.87 \pm 0.36	0.29 \pm 0.07*	0.44 \pm 0.32	0.35 \pm 0.08	0.10	0.36
	Ps MAR (μ m/day)	0.50 \pm 0.15	n.d.*	0.11 \pm 0.09	n.d.	0.01	0.13
	Ps BFR/BPm (μ m ² / μ m/day)	0.08 \pm 0.03	n.d.	0.01 \pm 0.009	n.d.	0.13	0.26
	Ps MPm/BPm (%)	0.17 \pm 0.04	0.008 \pm 0.008**	0.04 \pm 0.01	0.007 \pm 0.007*	0.003	0.04 S
	Ec MAR (μ m/day)	0.68 \pm 0.20	0.10 \pm 0.10*	0.35 \pm 0.20	n.d.*	0.01	0.26
	Ec BFR/BPm (μ m ² / μ m/day)	0.65 \pm 0.45	n.d.	0.02 \pm 0.02	n.d.	0.27	0.30
	Ec MPm/BPm (%)	0.43 \pm 0.26	0.001 \pm 0.0009	0.08 \pm 0.02	0.03 \pm 0.02	0.22	0.40

Hindlimb unloading (HU, $n = 8$ per genotype), controls ($n = 6$ per genotype) genotype (geno), endocortical surface (Ec), periosteum (Ps), mineral apposition rate (MAR), mineralisation perimeter (MPm), bone formation rate (BFR), and bone perimeter (BPm). * $p < 0.05$ unpaired t test compared to sedentary group within periostin group; $p < 0.05$, $p < 0.01$, $p < 0.001$ unpaired *Postn*^{+/+} and *Postn*^{−/−} mice by post-hoc Fisher's PLSD following 2×2 ANOVA. \$ p interaction between HU and genotype < 0.05 , \$\$ $p < 0.01$. Bold data emphasize that P HU is < 0.05 .

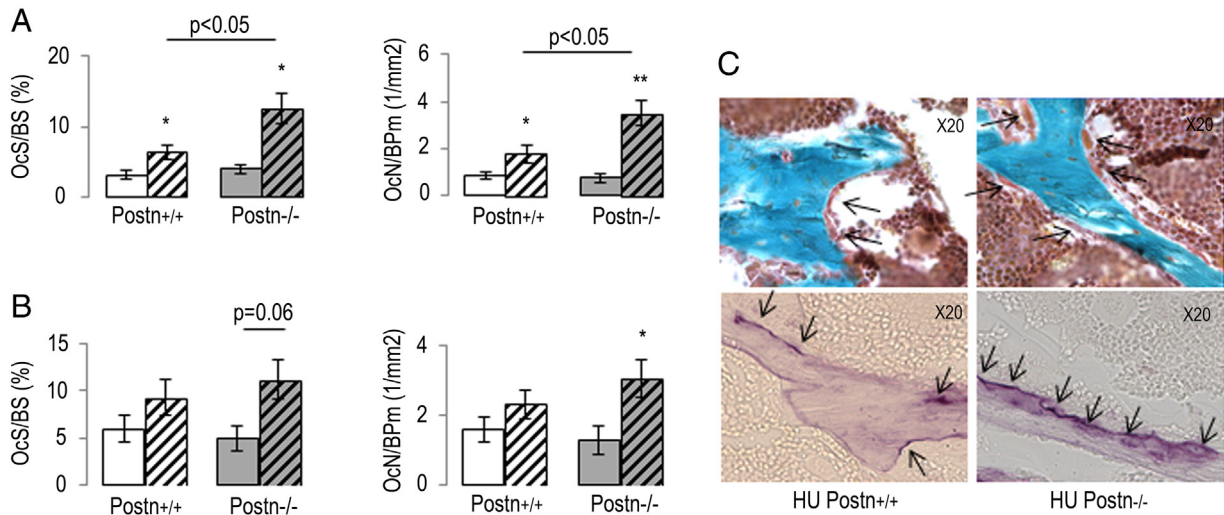


Fig. 3. Effects of 7 and 21 days of hindlimb unloading (HU) on osteoclast number and surfaces at trabecular bone surface in *Postn*^{+/+} and *Postn*^{-/-} mice. Bars show mean (\pm sem) measured after 7 days (A) or 21 days (B) of unloading (hatched bars) or sedentary (open bars) in *Postn*^{+/+} and *Postn*^{-/-} mice, respectively, white and gray bars. Osteoclast number (OcN), osteoclast surface (OcS), bone surface (BS), and bone perimeter (BPm). Images on right (C) show osteoclasts morphology and number revealed by Goldner staining (upper panels). Resorption activity (lower images) was revealed by Trap staining. * $p < 0.05$, ** $p < 0.01$ unpaired *t*-test compared to sedentary group within periostin group; $p < 0.05$ unpairing *Postn*^{+/+} and *Postn*^{-/-} mice by post hoc Fisher's PLSD following 2×2 ANOVA. $N = 8$ for HU groups and $n = 6$ for control groups.

further supported by the fact that *Sost*^{-/-} mice exhibit a strong up regulation of *Dkk1* vs. wild type littermate [27].

The bone reaction to unloading involves not only a decrease in bone formation but also an increase in bone resorption. More specifically, in the tail suspension model, the osteoclast number and/or surface are increased at an early time point and transiently [2,28]. Accordingly, we found an increase in osteoclast number after 7 days, which remained high but ceased to be significant after 21 days, correlating to the sclerostin expression profile. *In vitro* sclerostin has been shown to increase osteoclastogenesis through both an increase in *Rankl* and a decrease in *Opg* by inhibiting Wnt- β catenin signaling in osteocytes [29]. *In vivo*, the inhibition of skeletal deterioration in response to HU by sclerostin antibody has been demonstrated after short and long exposition of tail-suspension, i.e., 7, 14 and 21 days, arguing for a prevention effect through a decrease in bone resorption and then by maintaining bone formation [5,11,28,30]. Indeed, sclerostin neutralizing Ab inhibits bone resorption in different rodent models as well as in postmenopausal women [31,32]. In the absence of periostin, we observed a higher osteoclast number in HU vs. *Postn*^{+/+}, although it did not match the degradation in trabecular structure, which remained similar in *Postn*^{-/-} and *Postn*^{+/+}. We cannot exclude that with longer exposure to microgravity, BV/TV would have been more decreased in *Postn*^{-/-} HU compared to wild type since osteoclast number remains higher in HU vs. controls only in *Postn*^{-/-}. However, *Opg* and *Rankl* responded similarly to HU in *Postn*^{+/+} and *Postn*^{-/-} mice. Therefore, at this time, we can speculate firstly that periostin deficiency in osteoblast/osteocyte altered an anti-osteoclastic factor independent of *Opg*/*Rankl*/*Sost* [33]. We observed a higher expression of MMP13 in response to HU in *Postn*^{-/-} mice but not in *Postn*^{+/+} mice. Increase in MMP has been previously associated with osteocytic osteolysis, but this has been seen only in real microgravity condition (space shuttle mission) [34]. Secondly, periostin could have a direct role on osteoclasts as suggested by

in vitro studies [35–37]; however, to our knowledge this effect has never been demonstrated *in vivo*. In a previous study, we did not detect an effect of periostin deficiency on osteoclast numbers, surface or markers of bone resorption either in intact or ovariectomized mice [38]. Hence, these findings suggest an involvement of periostin in osteoclastogenesis only when this is triggered by mechanical stress.

There are several limitations to our study. First, we are discussing about changes in mRNA levels, which does not equate to protein expression. Second, mRNA was isolated from the whole diaphysis, which mainly contains both cortical and trabecular bone and therefore did not allow us to explain the differences in trabecular and cortical bone loss in *Postn*^{-/-} mice. Third, we did not use targeted knockout mice specifically in osteoblast or osteocyte, and therefore we were not able to appreciate in which cell periostin could impact as an anti-osteoclastic factor.

Notwithstanding, our data confirm a role of periostin in bone formation and highlight for the first time the involvement of periostin in the effects of hind limb suspension on cortical bone structure and strength through an increase in *Sost*. These results also would suggest that neutralizing periostin with a blocking antibody against this molecule or its receptor, α V β 5—which we previously showed to antagonize periostin effects on *in vitro* osteoblasts [15]—might prevent disuse-induced bone loss, similarly to sclerostin-neutralizing antibody [10,12]. More generally, these observations further support the central role of periostin in bone adaptation to mechanical loads, from microgravity to overload [39]. They may provide an additional mechanism to explain the effects of PTH on maintaining bone mass during immobilization/unloading, namely through its stimulation of periostin expression [15].

Supplementary data to this article can be found online at <http://dx.doi.org/10.1016/j.bone.2014.10.011>.

Acknowledgments

We thank Madeleine Lachize and Juliette Cicchini for their technical assistance. These studies were supported by ECTS-Amgen fellowship grant no ME8923 (to NB) and Swiss National Science Foundation grant no 3100A0-116633/1 (to SF) and Société Française de Rhumatologie (to MG). Authors's roles: Study design: NB and SF. Study conduct: MG and NB. Data analysis: MG and NB. Data interpretation: MG, NB, LV and SF. Drafting manuscript: MG and NB. Revising manuscript content and approving final version: MG, NB, LV and SF.

Table 3

Effects of 21 days of hindlimb unloading on osteoclastic gene expression in *Postn*^{+/+} and *Postn*^{-/-} mice.

Fold change expression vs controls	<i>Postn</i> ^{+/+} (n = 4)	<i>Postn</i> ^{-/-} (n = 4)
<i>Opg</i>	0.53 \pm 0.08	0.46 \pm 0.04
<i>Rankl</i>	1.80 \pm 0.14	1.77 \pm 0.21
<i>Mmp13</i>	0.83 \pm 0.08	1.46 \pm 0.06 *
<i>Trap</i>	1.27 \pm 0.09	1.54 \pm 0.06 *

* $p < 0.05$ unpaired *t* test compared to *Postn*^{+/+} mice.

References

- [1] Vico L, Lafage-Proust MH, Alexandre C. Effects of gravitational changes on the bone system in vitro and in vivo. *Bone* 1998;22(5 Suppl):955–1005.
- [2] Martin A, de Vittoris R, David V, Moraes R, Begeot M, Lafage-Proust MH. Leptin modulates both resorption and formation while preventing disuse-induced bone loss in tail-suspended female rats. *Endocrinology* 2005;146(8):3652–9.
- [3] Tatsumi S, Ishii K, Amizuka N, Li M, Kobayashi T, Kohno K, et al. Targeted ablation of osteocytes induces osteoporosis with defective mechanotransduction. *Cell Metab* 2007;5(6):464–75.
- [4] Robinson JA, Chatterjee-Kishore M, Yaworsky PJ, Cullen DM, Zhao W, Li C, et al. Wnt/beta-catenin signaling is a normal physiological response to mechanical loading in bone. *J Biol Chem* 2006;281(42):31720–8.
- [5] Lin C, Jiang X, Dai Z, Guo X, Weng T, Wang J, et al. Sclerostin mediates bone response to mechanical unloading through antagonizing Wnt/beta-catenin signaling. *J Bone Miner Res* 2009;24(10):1651–61.
- [6] Li X, Ominsky MS, Niu QT, Sun N, Daugherty B, D'Agostin D, et al. Targeted deletion of the sclerostin gene in mice results in increased bone formation and bone strength. *J Bone Miner Res* 2008;23(6):860–9.
- [7] Li X, Zhang Y, Kang H, Liu W, Liu P, Zhang J, et al. Sclerostin binds to LRP5/6 and antagonizes canonical Wnt signaling. *J Biol Chem* 2005;280(20):19883–7.
- [8] Robling AG, Niziolek PJ, Baldrige LA, Condon KW, Allen MR, Alam I, et al. Mechanical stimulation of bone in vivo reduces osteocyte expression of Sost/sclerostin. *J Biol Chem* 2008;283(9):5866–75.
- [9] Moriishi T, Fukuyama R, Ito M, Miyazaki T, Maeno T, Kawai Y, et al. Osteocyte network; a negative regulatory system for bone mass augmented by the induction of Rankl in osteoblasts and Sost in osteocytes at unloading. *PLoS One* 2012;7(6):e40143.
- [10] Tian X, Jee WS, Li X, Paszty C, Ke HZ. Sclerostin antibody increases bone mass by stimulating bone formation and inhibiting bone resorption in a hindlimb-immobilization rat model. *Bone* 2011;48(2):197–201.
- [11] Shahnazari M, Wronski T, Chu V, Williams A, Leeper A, Stolina M, et al. Early response of bone marrow osteoprogenitors to skeletal unloading and sclerostin antibody. *Calcif Tissue Int* 2012;91(1):50–8.
- [12] Spatz JM1, Ellman R, Cloutier AM, Louis L, van Vliet M, Suva LJ, et al. Sclerostin antibody inhibits skeletal deterioration due to reduced mechanical loading. *J Bone Miner Res* 2013;28(4):865–74.
- [13] Qin W, Sun L, Cao J, Peng Y, Collier L, Wu Y, et al. The central nervous system (CNS)-independent anti-bone-resorptive activity of muscle contraction and the underlying molecular and cellular signatures. *J Biol Chem* 2013;288(19):13511–21.
- [14] Bonnet N, Standley KN, Bianchi EN, Stadelmann V, Foti M, Conway SJ, et al. The extracellular matrix protein periostin is required for sclerostin inhibition and the anabolic response to mechanical loading and physical activity. *J Biol Chem* 2009;284(51):35939–50.
- [15] Bonnet N, Conway SJ, Ferrari SL. Regulation of beta catenin signaling and parathyroid hormone anabolic effects in bone by the extracellular matrix protein periostin. *Proc Natl Acad Sci U S A* 2012;109(37):15048–53.
- [16] Kramer I, Halleux C, Keller H, Pegurri M, Gooi JH, Weber PB, et al. Osteocyte Wnt/beta-catenin signaling is required for normal bone homeostasis. *Mol Cell Biol* 2010;30(12):3071–85.
- [17] Kühn B, del Monte F, Hajjar RJ, Chang YS, Lebeche D, Arab S, et al. Periostin induces proliferation of differentiated cardiomyocytes and promotes cardiac repair. *Nat Med* 2007;13(8):962–9.
- [18] Gillan L, Matei D, Fishman DA, Gerbin CS, Karlan BY, Chang DD. Periostin secreted by epithelial ovarian carcinoma is a ligand for alpha(V)beta(3) and alpha(V)beta(5) integrins and promotes cell motility. *Cancer Res* 2002;62(18):5358–64.
- [19] Shimazaki M, Nakamura K, Kii I, Kashima T, Amizuka N, Li M, et al. Periostin is essential for cardiac healing after acute myocardial infarction. *J Exp Med* 2008;205(2):295–303.
- [20] Rios H, Koushik SV, Wang H, Wang J, Zhou HM, Lindsley A, et al. Periostin null mice exhibit dwarfism, incisor enamel defects, and an early-onset periodontal disease-like phenotype. *Mol Cell Biol* 2005;25(24):11131–44.
- [21] Iida-Klein A, Lu SS, Yokoyama K, Dempster DW, Nieves JW, Lindsay R. Precision, accuracy, and reproducibility of dual X-ray absorptiometry measurements in mice in vivo. *J Clin Densitom* 2003;6(1):25–33.
- [22] Hildebrand T, Rueggeger P. A new method for the model-independent assessment of thickness in the three-dimensional images. *J Microsc* 1997;185:67–75.
- [23] Parfitt AM, Drezner MK, Glorieux FH, Kanis JA, Malluche H, Meunier PJ, et al. Bone histomorphometry: standardization of nomenclature, symbols, and units. Report of the ASBMR Histomorphometry Nomenclature Committee. *J Bone Miner Res* 1987;2(6):595–610.
- [24] Stansfield WE1, Andersen NM, Tang RH, Selzman CH. Periostin is a novel factor in cardiac remodeling after experimental and clinical unloading of the failing heart. *Ann Thorac Surg* 2009;88(6):1916–21.
- [25] Ruan K, Bao S, Ouyang G. The multifaceted role of periostin in tumorigenesis. *Cell Mol Life Sci* 2009;66(14):2219–30.
- [26] Kashima TG, Nishiyama T, Shimazu K, Shimazaki M, Kii I, Grigoriadis AE, et al. Periostin, a novel marker of intramembranous ossification, is expressed in fibrous dysplasia and in c-Fos-overexpressing bone lesions. *Hum Pathol* 2009;40(2):226–37.
- [27] Chang MK, Kramer I, Keller H, Gooi JH, Collett C, Jenkins D, et al. Reversing LRP5-dependent osteoporosis and SOST deficiency-induced sclerosing bone disorders by altering WNT signaling activity. *J Bone Miner Res* 2014;29(1):29–42.
- [28] Shahnazari M1, Kurimoto P, Boudignon BM, Orwoll BE, Bikle DD, Halloran BP. Simulated spaceflight produces a rapid and sustained loss of osteoprogenitors and an acute but transitory rise of osteoclast precursors in two genetic strains of mice. *Am J Physiol Endocrinol Metab* 2012;303(11):E1354–62.
- [29] Wijenayaka AR, Kogawa M, Lim HP, Bonewald LF, Findlay DM, Atkins GJ. Sclerostin stimulates osteocyte support of osteoclast activity by a RANKL-dependent pathway. *PLoS One* 2011;6(10).
- [30] Spatz JM, Ellman R, Cloutier AM, Louis L, van Vliet M, Suva LJ, et al. Sclerostin antibody inhibits skeletal deterioration due to reduced mechanical loading. *J Bone Miner Res* 2013;28(4):865–74.
- [31] Padhi D, Jang G, Stouch B, Fang L, Posvar E. Single-dose, placebo-controlled, randomized study of AMG 785, a sclerostin monoclonal antibody. *J Bone Miner Res* 2011;26(1):19–26.
- [32] McClung MR, Grauer A, Boonen S, Bolognese MA, Brown JP, Diez-Perez A, et al. Romosozumab in postmenopausal women with low bone mineral density. *N Engl J Med* 2014;370(5):412–20.
- [33] Grimston SK1, Goldberg DB, Watkins M, Brodt MD, Silva MJ, Civitelli R. Connexin43 deficiency reduces the sensitivity of cortical bone to the effects of muscle paralysis. *J Bone Miner Res* 2011;26(9):2151–60.
- [34] Blaber EA, Dvorochkin N, Lee C, Alwood JS, Yousuf R, Pianetta P, et al. Microgravity induces pelvic bone loss through osteoclastic activity, osteocytic osteolysis, and osteoblastic cell cycle inhibition by CDKN1a/p21. *PLoS One* 2013;8(4):e61372.
- [35] Nakamura I, Pilkington MF, Lakkakorpi PT, Lipfert L, Sims SM, Dixon SJ, et al. Role of alpha(v)beta(3) integrin in osteoclast migration and formation of the sealing zone. *J Cell Sci* 1999;112:3985–93.
- [36] Merle B, Garnero P. The multiple facets of periostin in bone metabolism. *Osteoporos Int* 2012;23(4):1199–212.
- [37] Merle B, Bouet G, Rousseau JC, Bertholon C, Garnero P. Periostin and transforming growth factor beta-induced protein (TGFbeta) are both expressed by osteoblasts and osteoclasts. *Cell Biol Int* 2014;38(3):398–404.
- [38] Bonnet N, Lesclous P, Saffar JL, Ferrari S. Zoledronate effects on systemic and jaw osteopenias in ovariectomized periostin-deficient mice. *PLoS One* 2013;8(3):e58726.
- [39] Bonnet N, Gineys E, Ammann P, Conway SJ, Garnero P, Ferrari S. Periostin deficiency increases bone damage and impairs injury response to fatigue loading in adult mice. *PLoS One* 2013;8(10):e78347.